University of Iceland
Faculty of Physical Sciences

He^+ and Xe^+ velocities near the presheath-sheath boundary in a He/Xe discharge

by

Davíð Ingvi Snorrason

16 ECTS thesis submitted in partial fulfillment of a B.Sc. degree in Engineering Physics at the University of Iceland

Advisor
Dr. Jón Tómas Guðmundsson

Reykjavík
February, 2017

He^+ and Xe^+ velocities near the presheath-sheath boundary in a He/Xe discharge
16 ECTS thesis submitted in partial fulfillment of a B.Sc.degree in Engineering Physics at the University of Iceland

Faculty of Physical Sciences
School of Engineering and Natural sciences
University of Iceland
Dunhagi 5
107, Reykjavík
Iceland
Telephone: 525 4000

Bibliographic information:
Davíð Ingvi Snorrason, 2017, He^+ and Xe^+ velocities near the presheath-sheath boundary in a He/Xe discharge, B.Sc. thesis, Faculty of Physical Sciences, University of Iceland.
ISBN XX

Printing: Háskólaprent, Fálkagata 2, 107 Reykjavík
Reykjavík, Iceland, February 2017

Abstract

The oopd1 particle-in-cell Monte Carlo collision (PIC-MCC) code is used to simulate He/Xe discharge in order to determine the velocities of helium and xenon ions at the presheath-sheath boundary in two ion species plasmas. Nine cases were simulated, seven of which are He/Xe mixtures with varying helium partial pressure and then two cases, one for pure helium and one pure xenon, while the discharge pressure is kept at 0.7 mTorr. As the partial pressure of helium is increased the velocities at the presheath-sheath boundary also increase for both ion species. In all cases the xenon ions reach the presheath-sheath boundary at approximately their own sound speed and the helium ions reach the boundary at a velocity which is much lower than their sound speed.

Introduction

The velocities of ions in a two ion plasma mixture continues to be of interest in plasma physics. The question of how the velocities of ions are determined at the presheath-sheath boundary in plasmas with multiple-ion species is a fundamental question in basic physics. In weakly collisional, single-ion plasmas the ions are accelerated to its sound speed u_{B} in the presheath. The ions are thus expected to have attained their sound speed at the sheath-presheath boundary according to the Bohm criterion [1]

$$u_{\mathrm{B}} = \left(\frac{eT_e}{M_i}\right)^{1/2} \tag{1}$$

where e is the elementary charge, T_e is the electron temperature in Volts and M_i is the mass of the ions species in the plasma. For a plasma system where two or more ion species are present the ions at the sheath-presheath boundary must satisfy the general Bohm criterion [2].

$$1 \geq \sum_j \frac{n_j c_j^2}{n_e v_j^2} \tag{2}$$

where the sum is taken over the number of different ion-species where n_j is the ion density, n_e is the electron density, c_j is the velocity of sound of each ion species and v_j is the drift velocity of individual ion species and the electrons are assumed to have Maxwellian electron energy distribution. This criterion however remains unclear for plasmas that contain multiple ion species as there are an infinite number of solutions. There are two simple solutions that are of fundamental interest. These solutions however suggest two very different outcomes. The first would be that in a multi-ion-species plasma the ions reach the sheath-presheath boundary at a common velocity, that is, the ion sound speed of the system. The latter solution suggests that each ion species in the system reaches it's individual Bohm velocity, or sound speed.

The issue of the ion velocities at the pre-sheath - sheath edge has been explored experimentally by Lee et al. [3, 4] who applied laser-induced fluorescence (LIF) using two diode lasers in Ar/Xe plasma to measure the argon and xenon ion velocity distribution near a negatively biased plate. They concluded that the Ar^+ and Xe^+-ion velocities near the sheath-presheath boundary approach the common ion sound speed in the discharge and thus satisfy the generalized Bohm criterion. Thus, argon ions reach the sheath edge travelling faster and xenon ions travelling slower than the single-ion Bohm speed, both ions travel at a speed very close to the ion sound speed of the system. Similar

findings have been reported for Ar/He plasma where the Ar-ions reach the presheath-sheath boundary travelling faster than their individual Bohm velocities [5] and for He/Xe plasma [6] where the helium ion velocity approaches the common sound speed of the system. Furthermore, when the relative concentration differences deviate from roughly equal concentration each species approaches its own Bohm velocity [7]. There have been reports of instabilities and its magnitude peaks near the sheath edge, and thus identified as two-stream instability, observed in Ar/Xe [6], Xe/He [6], Ar/He [8] and Ar/Xe/Kr [9] plasmas. However, in a He/Xe plasma instability was only observed when helium ions are the majority [6]. Particle-in-cell Monte Carlo collision (PIC/MCC) simulations have shown that each ion in an Ar/Xe plasma reaches its own Bohm velocity at the presheath-sheath interface [10] and thus contradict the experimental findings of Lee et al. [3, 4]. However it has been pointed out by Hershkowitz et al [11] that there is substantial evidence (both experimental and theoretical) that Coulomb collisions and ion-ion beam instabilities are important in these plasmas, but neither effect is included in these earlier simulations [10]. Here we explore the ion velocities at the presheath-sheath boundary in a He/Xe discharge using PIC/MCC simulations. We compare the results of the simulation to recent experimental rsults on the He/Xe discharge.

The He/Xe system

The plasma systems simulated were set up with the goal of exploring the positive ion velocities at the presheath-sheath boundary and thus determine which solution of equation (2) is valid. For He and Xe there is a great difference in the masses of the ion species and helium has very high ionization potential which is expected to lead to relatively high electron temperature. Both of these are expected to be preferable to promote ion-ion two stream instability [12]. Indeed instabilities have been observed experimentally in the He/Xe discharge [6]. The partial-pressures range from pure helium to pure xenon in steps of 0.1 mTorr, aside from one where the pressures contribution is equal, keeping the total pressure of the system at 0.7 mTorr in all cases. These systems are simulated using the PIC/MCC collision method. We use the one-dimensional object-oriented PIC/MCC code `oopd1` [13, 14] and here it is applied to study the ion velocities at the sheath edge for a discharge in a mixture of helium and xenon. This method models the behaviour of the plasma by solving the Poisson equation for each collision of super-particles.The simulation attempts to model the multidipole experimental configuration described by Lee et al. [3, 4] and by Herskowitz et al [6]. The simulated discharge is maintained between two equal-area electrodes $(1.77 \times 10^{-2}\mathrm{m}^2)$ separated by a gap of 10 cm. The left hand electrode is biased at -30V to generate an ion sheath. To model the ionization created by energetic electrons in a multidipole chamber, we use a volume source with a uniform ionization rate of $4.3 \times 10^{-19}\mathrm{m}^{-1}\mathrm{s}^{-1}$ to maintain the steady state. The electrons are created with electron temperature of 88 eV. The electron temperature affects the velocity of the particles in the system and subsequently the velocity they reach at the sheath-presheath boundary. The simulation grid is uniform and consists of 2000 cells. Approximately 350,000 super-particle electrons and positive ions were used in the simulations. The electron time step is chosen to be 3.6×10^{-11} s. The simulations were run to a steady state and diagnostics were gathered over 5,500,000 time steps.

The reaction sets and cross-sections used in the simulation are a collection from various sources. The reaction set for xenon is the same as used in earlier simulation [10]. The cross section for *e*-Xe elastic scattering is from the work of Mozumder [15]. The cross section for electron impact ionization is taken from from Rapp et al [16]. The cross section for Xe-Xe elastic scattering comes from theoretical work by Phelps [17]. The cross sections for electron impact excitation of Xenon to the metastable states $3^{0,2}$P at a threshold of 8.315 eV, higher states at 9.570 eV and to radiative states 3^1P at a threshold of 8.47eV [18]. The reaction set for xenon and references to cross sections

used are given in table I. The cross section for *e*-He elastic scattering is assembled from three sources [19–21]. The cross section for He-He elastic scattering come from two sources [17, 22]. The cross sections for elastic ion scattering and resonant charge exchange He + $He^+ \rightarrow$ He + He^+ comes from the collection of Phelps [17]. Due to earlier criticism [11] the ion-ion Coulomb collisions have been added to the reaction set. The cross sections for ion-ion Coulomb collisions (Xe^+-Xe^+ and He^+-He^+) are estimated by

$$\sigma = \Big(\frac{m_1 + m_2}{m_2}\Big)\pi b_0^2 \ln\Lambda \tag{3}$$

[23] where m_1 and m_2 refer to the masses of the two colliding species with $m_2 < m_1$, $b_0 = e/(4\pi\epsilon_0\varepsilon_R)$ is the classical distance of closest approach where ε_R is the center-of-mass energy in eV and $\ln\Lambda = \ln(2\lambda_{De}/b_0)$ where $\lambda_{\rm De}$ is the Debye length for electrons. For He there are various excitation metastable states included in the reaction set, firstly those that are excited by electrons from the ground state, those are 2^3S at 19.82 eV, 2^1S at 20.62 eV, 2^3P at 20.97 and 2^1P at 21.22 eV. Secondly there are electron excitations from the metastable states to higher energy states, those are $2^1S \rightarrow 2^3P$ at 0.348 eV, $2^1S \rightarrow 2^1P$ at 0.604 eV, $2^3S \rightarrow 2^1S$ at 0.796 eV, $2^3S \rightarrow 2^3P$ at 1.148 eV and $2^3S \rightarrow 2^1P$ at 1.404 eV. Helium-electron de-excitation reactions are also included in the calculations, those are $2^1S \rightarrow 2^3S$, $2^3P \rightarrow 1^1S$, $2^1P \rightarrow 1^1S$, $2^3S \rightarrow 1^1S$ and $2^1S \rightarrow 1^1S$. The *e*-He impact ionizations from metastable states included are $1^1S \rightarrow He^+$, $^3S_2 \rightarrow He^+$ and $2^1S \rightarrow He^+$ [24]. The cross sections for spontaneuos emission are included, those are $2^3P \rightarrow 2^3S$, $2^1P \rightarrow 2^1S$ and $2^1P \rightarrow 1^1S$ [25]. The reaction set for helium and references to the source for the cross sections used are given in table II. The cross sections for charge exchange between helium and xenon He^+ + Xe $\rightarrow$ He^+ + Xe is assumed to be the average of the cross sections for the charge exchange between Xe^+ + Xe and He^+ + He. The cross section for Xe^+ + He $\rightarrow$ Xe^+ + He elastic scattering is considered to be the same as for He^+ + He $\rightarrow$ He^+ + He [26]. The cross section for He + Xe $\rightarrow$ He + Xe elastic scattering is taken as the average of cross sections for Xe-Xe and He-He. The reaction set for the cross terms between helium and xenon is given in table III.

Table I: The reaction set for a xenon discharge.

Reaction	Process	Reference
$e + Xe \longrightarrow e + Xe$	elastic electron scattering	[15]
$e + Xe \longrightarrow e + Xe^{m}$	electron impact excitation to metastable states (8.315 eV)	[18]
$e + Xe \longrightarrow e + Xe^{r}$	electron impact excitation to radiative states (8.437 eV)	[18]
$e + Xe \longrightarrow e + Xe^{h}$	electron impact excitation to higher levels (9.570 eV)	[18]
$e + Xe \longrightarrow Xe^{+} + 2e$	electron impact ionization (12.13 eV)	[16]
$Xe + Xe \longrightarrow Xe + Xe$	elastic neutral scattering	[27]
$Xe^{+} + Xe^{+} \longrightarrow Xe^{+} + Xe^{+}$	ion-ion Coulomb collision	
$Xe + Xe^{+} \longrightarrow Xe + Xe^{+}$	elastic ion scattering and resonant charge exchange	[28]

Table II: The reaction set for a helium discharge.

Reaction	Process		Reference
$e + He \longrightarrow e + He$	elastic electron scattering		[19–21]
$e + He(1\ ^1S) \longrightarrow e + He(2\ ^3S)$	excitation from GS to metastable state 2^3S (19.82 eV)		[24]
$e + He(1\ ^1S) \longrightarrow e + He(2\ ^1S)$	excitation from GS to metastable state 2^1S (20.62 eV)		[24]
$e + He(1\ ^1S) \longrightarrow e + He(2\ ^3P)$	excitation from GS to 2^3P (20.97 eV)		[24]
$e + He(1\ ^1S) \longrightarrow e + He(2\ ^1P)$	excitation from GS to 2^1P (21.22 eV)		[24]
$e + He(2\ ^3S) \longrightarrow e + He(2\ ^3P)$	excitation from 2^3S to 2^3P (1.148 eV)		[24]
$e + He(2\ ^3S) \longrightarrow e + He(2\ ^1P)$	excitation from 2^3S to 2^1P (1.404 eV)		[24]
$e + He(2\ ^1S) \longrightarrow e + He(2\ ^3P)$	excitation from 2^1S to 2^3P (0.348 eV)		[24]
$e + He(2\ ^1S) \longrightarrow e + He(2\ ^1P)$	excitation from 2^1S to 2^1P (0.604 eV)		[24]
$e + He(2\ ^3S) \longrightarrow e + He(2\ ^1S)$	excitation from 2^3S to 2^1S (0.796 eV)		[24]
$e + He(2\ ^1S) \longrightarrow e + He(2\ ^3S)$	de-excitation from detailed balancing on 2^1S to 2^3S		[24]
$e + He(2\ ^3P) \longrightarrow e + He(1\ ^1S)$	de-excitation from detailed balancing on 2^3P to GS		[24]
$e + He(2\ ^1P) \longrightarrow e + He(1\ ^1S)$	de-excitation from detailed balancing on 2^1P to GS		[24]
$e + He(2\ ^3S) \longrightarrow e + He(1\ ^1S)$	de-excitation from detailed balancing on 2^3S to GS		[24]
$e + He(2\ ^1S) \longrightarrow e + He(1\ ^1S)$	de-excitation from detailed balancing on 2^1S to GS		[24]
$e + He(1\ ^1S) \longrightarrow He^{+} + 2e$	electron impact ionization from GS (24.59 eV)		[29]
$e + He(2\ ^3S) \longrightarrow He^{+} + 2e$	electron impact ionization from 2^3S (4.76 eV)		[24]
$e + He(2\ ^1S) \longrightarrow He^{+} + 2e$	electron impact ionization from 2^1S (3.97 eV)		[24]
$He + He \longrightarrow He + He$	elastic neutral scattering		[22, 27]
$He^{+} + He^{+} \longrightarrow He^{+} + He^{+}$	ion-ion Coulomb collision		
$He + He^{+} \longrightarrow He + He^{+}$	elastic ion scattering		[26]
$He + He^{+} \longrightarrow He^{+} + He$	charge exchange		[26], [30]
$He(2\ ^3P) \longrightarrow He(2\ ^3S) + h\nu$	spontaneous emission to 2^3S	$1 \times 10^{7}s^{-1}$	[31]
$He(2\ ^1P) \longrightarrow He(2\ ^1S) + h\nu$	spontaneous emission to 2^1S	$2.6 \times 10^{6}s^{-1}$	[31]
$He(2\ ^1P) \longrightarrow He(1\ ^1S) + h\nu$	spontaneous emission to GS	$1.8 \times 10^{9}s^{-1}$	[31]

Table III: The reaction set for the cross terms between xenon and helium

Reaction	**Process**	**Reference**
$He + Xe \longrightarrow He + Xe$	elastic neutral scattering	
$He + Xe^+ \longrightarrow He + Xe^+$	elastic ion scattering	[26]
$He^+ + Xe \longrightarrow He^+ + Xe$	elastic ion scattering	
$He^+ + Xe \longrightarrow He + Xe^+$	non-resonant charge exchange	

Determination of the sheath edge

The method used to accurately determine the location of the boundary between the pre-sheath and sheath is one of the methods described by Baalrud et al [32]. Beginning at the biased plate we calculate the normalized charge density

$$\rho = (n_i - n_e)/n_i \tag{4}$$

where n_i is the number of ions of a given species, n_e is the number of electrons, and working our way in we find the location where this value is as close to zero as possible. We use the criterion that ρ has to be less than 0.0000001. With this we could assume that moving closer to the biased plate from this point the plasma would no longer be quasi-neutral as there will be far less electrons present. After locating the presheath-sheath edge we look at velocity data from the simulation and obtain the velocity of the ions that are present at the presheath-sheath edge. This is demonstrated in figure 1 which shows the density profiles of the He^+ and Xe^+ -ions and electrons over the distance from the biased electrode for a discharge with helium and xenon partial pressures 0.6 and 0.1 mTorr, respectively. The electron density profile is also shown in the figure. We see that the electron density drops sharply as we approach the electrode. The sheath edge is indicated with a vertical dashed line. These values can then be compared to velocity values calculated using the Bohm criterion (equation(1)) and the electron temperature read from at the center of the simulated system.

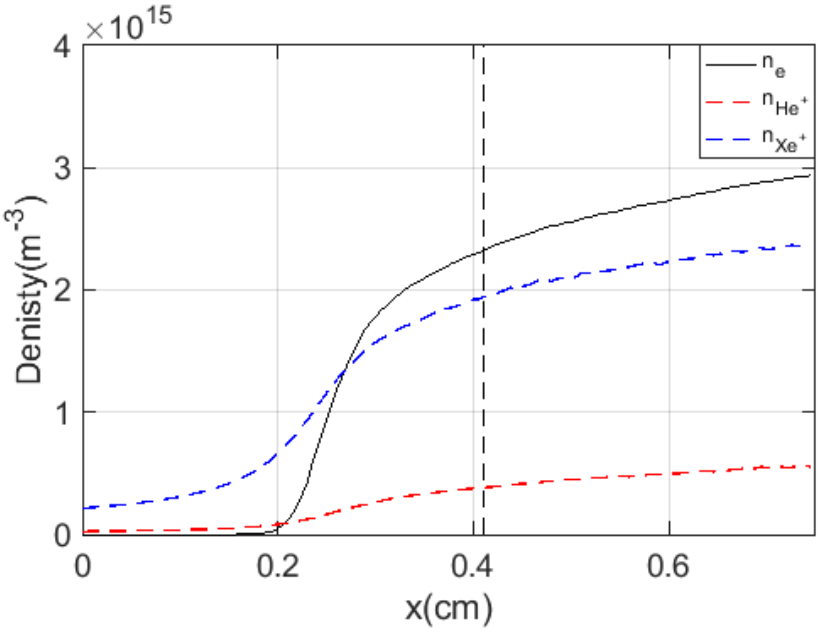

Figure 1: The density of He^+ and Xe^+-ions as a function of location relative to the biased electrode. The sheath edge is marked with a vertical dashed line.

Results and discussion

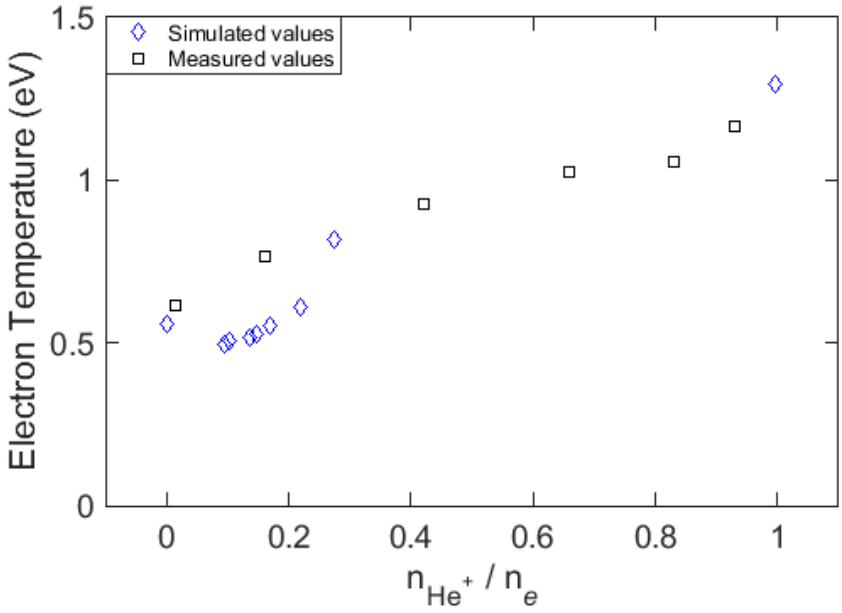

Figure 2: Final electron temperature from the simulation at the discharge center as blue diamonds and for comparison, measured electron temperature values [6] in a He/Xe plasma as black boxes, versus the He^+-ion fraction.

Figure 2 shows the discharge center electron temperature versus He^+-ion fraction for the various simulated cases. We compare the results from the simulation to the measured values from Hershkowitz et al [6]. We see that the electron temperature increases with increased He^+-ion fraction. The electron temperature is 0.5 eV for pure a Xe discharge and increases to 1.2 eV for a pure He discharge. We also see that there is a good agreement between the measured and simulated values at lower He^+-ion concentrations as well as pure helium plasma. In fact the value of 88 eV for the created electrons is chosen to get the simulated electron temperature close to the experimental findings.

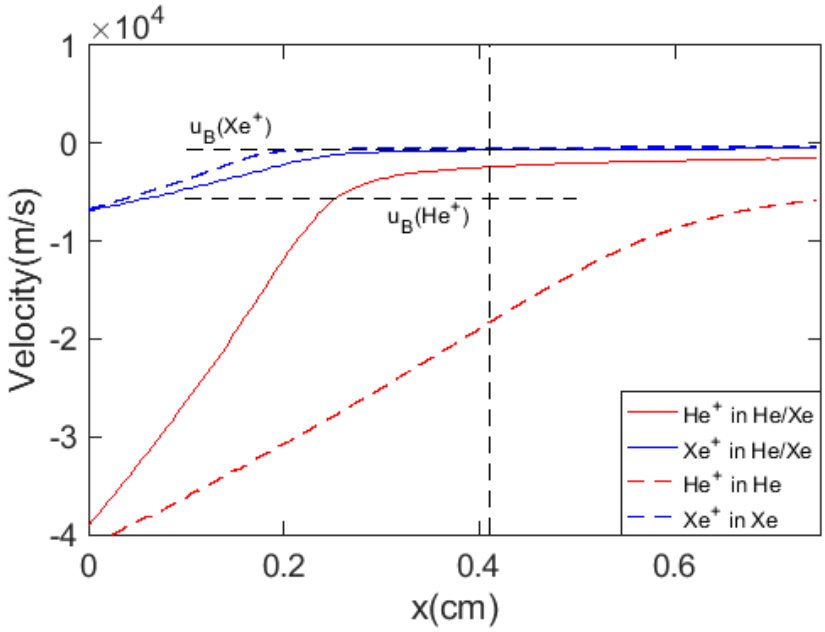

Figure 3: Velocity of helium and xenon ions over the distance from the biased base plate in the simulated chamber for a pure He discharge, a pure Xe discharge and a He/Xe discharge at 0.7 mTorr. In the helium-xenon discharge the partial pressures were 0.6 and 0.1 mTorr, respectively.

Figure 3 shows the velocity of He^+ and Xe^+-ions as a function of distance from the biased plate. In figure 3 the vertical dashed line shows the location of the presheath-sheath boundary in the two species plasma and the solid horizontal lines mark the velocity of each ion species of the single ion species plasmas calculated using the center electron temperature and the Bohm criterion (equation(1)). The solid red and blue lines show the velocity of He^+ and Xe^+-ions in a two ion species plasma whilst the dashed red and blue lines show the velocities of helium and xenon-ions where only one species is present. Comparing the velocity profiles we see that the xenon-ion velocities are quite similar in the mixture and pure cases, there is however a striking difference when we look at the helium-ion velocity profiles where the velocities in the pure case are significantly higher than those in the two species mixture.

Figure 4 shows the drift velocities of helium and xenon at the sheath-edge simulated using PIC/MC as well as the values for the velocity calculated using the electron tem-

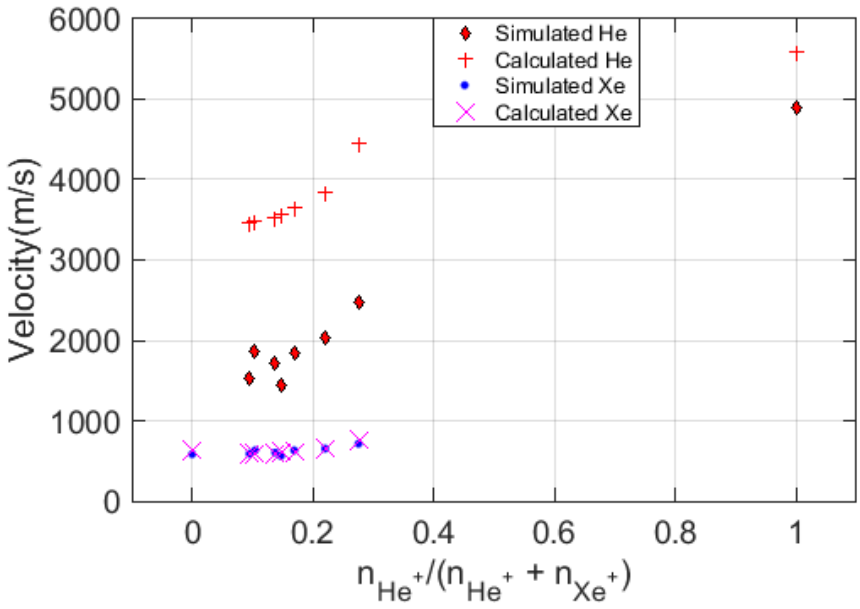

Figure 4: The drift velocity of helium and xenon ions at the sheath edge obtained from particle-in-cell Monte Carlo method, diamonds for helium and dots for xenon. Also shown are the velocities calculated using the electron temperature of the system and the Bohm criterion, crosses for helium and x's for xenon. These values are plotted against the number of helium ions realative to total number of ions present.

perature from the simulation. In the He/Xe mixtures the velocities of the helium ions obtained from the simulations are consistently much lower than the values calculated using the center electron temperature and the Bohm criterion (equation (1)), this does however not apply to the xenon ions. For the xenon the values match up quite closely to the values found using the Bohm criterion (equation(1)) and so in that case the Bohm-criterion gives a good prediction for the velocity at the sheath edge. In figure 4 we see that there is a large drop in the velocity of the helium ions when we compare the simulated values for the single species helium plasma and the two species helium-xenon plasma. For helium ions the values calculated using the Bohm-criterion are in most cases close to two times higher than the values optained from the simulation. The one exception is in the case where no xenon is present, where the velocity values for helium calculated using the Bohm-criterion and the simulation only differ by about 12 percent. The result is similar for pure xenon where the difference between the values is close to

7.5 percent. We see in figures 4 and 5 that the velocity of the Xe^+-ions is quite stable compared with the velocity of He^+-ions when the number of ions present, from each species, is changed. The velocity of the xenon ions goes from about 605m/s to about 722 m/s which is close to a 20 percent increase, this happens as the ratio of xenon ions present is decreasing. The change in the helium ion velocity is a bit more erratic but as the ratio of helium ions increases, so does their velocity, which goes from 1534 m/s to 2470 m/s which is an increase of about 61 percent. The velocity of both ion species increases as the helium partial pressure increases.

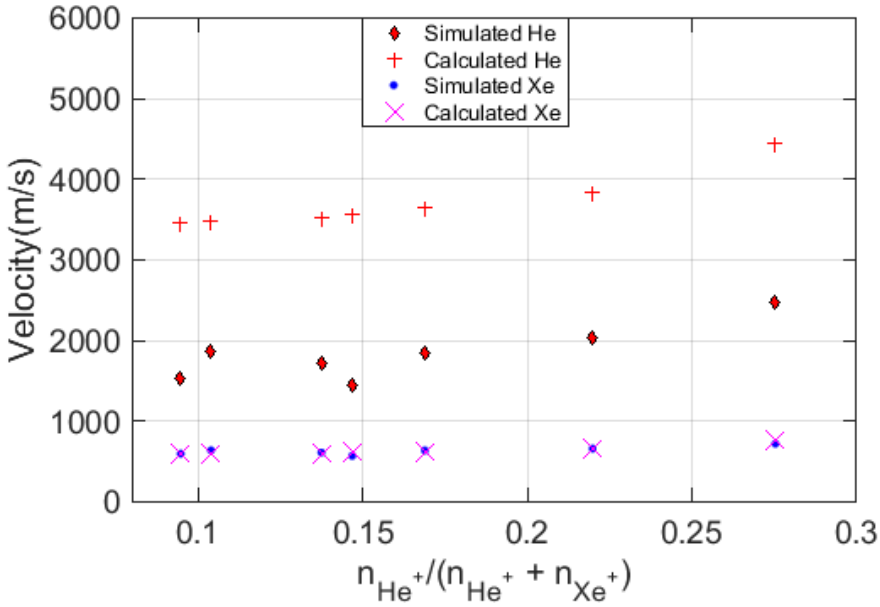

Figure 5: The drift velocity of He^+ and Xe^+ ions at the sheath edge obtained from particle-in-cell Monte Carlo method, diamonds for helium and dots for xenon. Also shown are the velocities calculated using the electron temperature of the system and the Bohm criterion, crosses for helium and x's for xenon. These values are plotted against the number of helium ions relative to total number of ions present. This figure only shows the values for two-species plasma.

In figure 5 we look at the n_{He^+} fraction up to 0.3 and we see more clearly the simulated velocity values from the cases where both helium and xenon -ion species are present. We can see more clearly the increase in velocity of the Xe^+-ions when the He^+-ion concentration is increased. The velocity increase for the xenon-ions is somewhat small compared to the increase in velocity of the helium-ions.

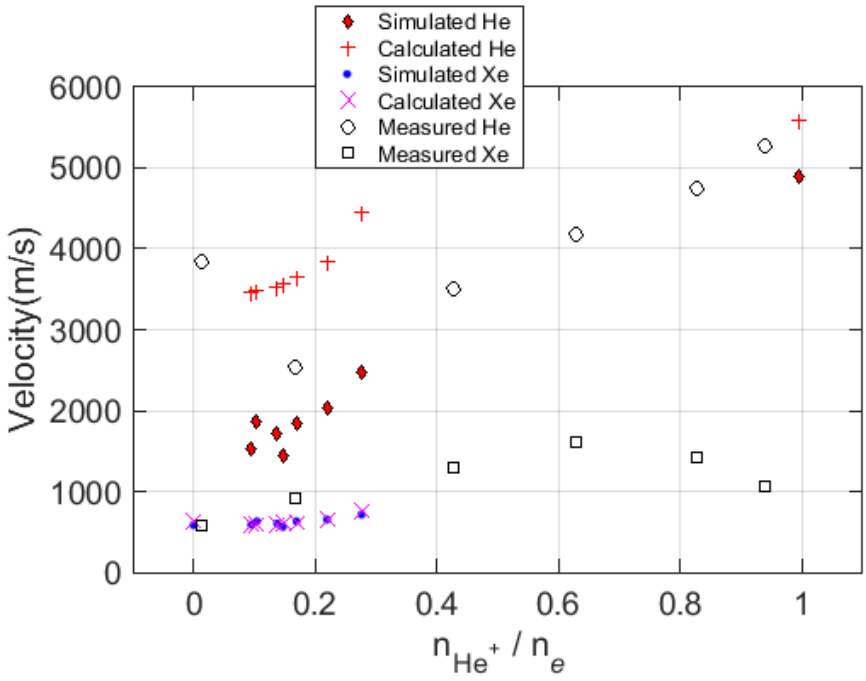

Figure 6: The drift velocity of helium and xenon ions at the sheath edge obtained from particle-in-cell Monte Carlo method, diamonds for helium and dots for xenon. Velocities calculated using the electron temperature of the system and the Bohm criterion are also marked, crosses for helium-ions and x's for xenon-ions. Also plotted are values taken from [6] which are marked with asterix's for He^+-ions and squares for Xe^+-ions. These values are plotted against the number of He^+-ions relative to the number of electrons.

In figure 6 measured velocity values [6] from a Xe-He mixture have been added to the graph. We see an agreement in the way that the velocities of the ions increase with increased relative He^+-ion density. This seems to have a somewhat greater effect on the helium-ions as we see from the more drastic changes in velocity of those ions. As the ratio of helium-ions present in the mixture is increased the helium-ion velocity also increases significantly. In fact Herskowitz et al [6] show that the He^+-ion velocity follows the common sound speed of the He/Xe system. We also see that the measured velocities for Xe^+-ions agree well with the results from the simulations at least for low He^+-ion concentration. Similarly the measured He^+-ion velocity agrees well with the results from the simulations. There is however a data point for the helium-ions taken from [6] when the $n_{\mathrm{He}^+}/n_{\mathrm{e}}$ is quite close to zero that goes against this development. In all cases the xenon ions reach presheath-sheath boundary at approximately their own sound speed while the helium ions reach the boundary at a velocity that is much lower than its sound speed.

Conclusions

PIC/MCC simulation was performed on a He/Xe discharge in order to explore the ion velocities of positive ions at the presheath-sheath boundary. We find good agreement between the measured He^+-ion velocity values from Hershokwitz et al [6] and the values obtained from the simulation. Similarly the velocity of Xe^+-ions found by simulation agrees with experimental findings. We can also see that the Xe^+-ions reach the presheath-sheath boundary at its individual sound speed, while the He^+ reach the boundary at a much lower velocity than its individual sound speed.

[1] D. Bohm, in *The characteristics of electrical discharges in magnetic fields*, edited by A. Guthrie and R. K. Wakerling (McGraw-Hill, New York, 1949), no. I, volume 5 in National nuclear energy series – Manhattan project technical section, chap. 3, pp. 77–86.
[2] K.-U. Riemann, IEEE Transactions on Plasma Science **23**, 709 (1995).
[3] D. Lee, G. Severn, L. Oksuz, and N. Hershkowitz, Journal of Physics D: Applied Physics **39**, 5230 (2006).
[4] D. Lee, N. Hershkowitz, and G. D. Severn, Applied Physics Letters **91**, 041505 (2007).
[5] G. D. Severn, X. Wang, E. Ko, and N. Hershkowitz, Physical Review Letters **90**, 145001 (2003).
[6] N. Hershkowitz, C.-S. Yip, and G. D. Severn, Physics of Plasmas **18**, 057102 (2011).
[7] C.-S. Yip, N. Hershkowitz, and G. Severn, Physical Review Letters **104**, 225003 (2010).
[8] N. Hershkowitz, Physics of Plasmas **12**, 055502 (pages 11) (2005).
[9] C.-S. Yip, N. Hershkowitz, G. Severn, and S. D. Baalrud, Physics of Plasmas p. 050703 (2016).
[10] J. T. Gudmundsson and M. A. Lieberman, Physical Review Letters **107**, 045002 (2011).
[11] N. Hershkowitz, G. D. Severn, S. D. Baalrud, C. C. Hegna, and J. D. Callen, Physical Review Letters **108**, 139501 (2012).
[12] S. D. Baalrud and C. C. Hegna, Physics of Plasmas **18**, 023505 (2011).
[13] J. Hammel and J. P. Verboncoeur, Bulletin of the American Physical Society **48**, 66 (2003).
[14] J. P. Verboncoeur, A. B. Langdon, and N. T. Gladd, Computer Physics Communications **87**, 199 (1995).
[15] A. Mozumder, Journal of Chemical Physics **72**, 6289 (1980).
[16] D. Rapp and P. Englander-Golden, Journal of Chemical Physics **43**, 1464 (1965).
[17] A. V. Phelps, URL http://jilawww.colorado.edu/~avp/collision_data/neutralneutral/atomatom.txt.
[18] Y. Sakai, S. Sawada, and H. Tagashira, Journal of Physics D: Applied Physics **24**, 283 (1991).
[19] M. J. Brunger, S. J. Buckman, L. J. Allen, I. E. McCarthy, and K. Ratnavelu, Journal of Physics B: Atomic, Molecular and Optical Physics **25**, 1823 (1992).
[20] M. Vinodkumar, C. Limbachiya, B. Antony, and K. N. Joshipura, Journal of Physics B: Atomic, Molecular and Optical Physics **40**, 3259 (2007).
[21] H. H. Michels, F. E. Harris, and R. M. Scolsky, Physics Letters A **28**, 467 (1969).
[22] R. Feltgen, H. Pauly, F. Torello, and H. Vehmeyer, Physical Review Letters **30**, 820 (1973).
[23] M. A. Lieberman and A. J. Lichtenberg, *Principles of Plasma Discharges and Materials Processing* (John Wiley & Sons, New York, 2005), 2nd ed.

[24] Y. Ralchenko, R. Janev, T. Kato, D. V. Fursa, I. Bray, and F. de Heer, Atomic Data and Nuclear Data Tables **94**, 603 (2008).

[25] W. Wiese and J. Fuhr, Journal of Physical and Chemical Reference Data **38**, 565 (2009).

[26] W. H. Cramer and J. H. Simons, Journal of Chemical Physics **26**, 1272 (1957).

[27] A. V. Phelps, Tech. Rep. JILA Information Center Report 28, University of Colorado at Boulder (1985), URL http://jilawww.colorado.edu/~avp/collision_data/electronneutral/electron.txt.

[28] D. Piscitelli, A. V. Phelps, J. de Urquijo, E. Basurto, and L. C. Pitchford, Physical Review E **68**, 046408 (2003).

[29] R. Rejoub, B. G. Lindsay, and R. F. Stebbings, Physical Review A **65**, 042713 (2002).

[30] A. Galli, A. Giardini-Guidoni, and G. G. Volpi, Journal Il Nuovo Cimento **26**, 845 (1962).

[31] H. H. Michels, F. E. Harris, and R. M. Scolsky, Physics Letter A **28**, 467 (1969).

[32] S. D. Baalrud, B. Scheiner, B. Yee, M. Hopkins, and E. Barnat, Plasma Physics and Controlled Fusion **57**, 044003 (2015).